AUT Journal of Electrical Engineering

AUT J. Electr. Eng., 56(3) (2024) 407-418
DOI: 10.22060/eej.2024.23101.5588

Analytical Modeling of GaN-HEMT Considering Finite Width of Two-Dimensional Electron Gas

Behnam Jafari Touchaei, Majid Shalchian

Department of Electrical Engineering, Amirkabir University of Technology (Tehran Polytechnique), Tehran, Iran

ABSTRACT: In this work, we present an analytical DC model for the Gallium Nimtide High Electron Mobility Transistor by taking into account the finite width of the two-dimensional electron gas (2DEG) layer. The model predicts the vertical electric field in the device, especially at the interface of AlGaN and GaN layers, electrostatic potential, and energy band diagram are also obtained by the model. The general form of Gauss's law including piezoelectric and spontaneous polarization effect is employed to obtain this model in different regions from top to bottom of the GaN-HEMT. The model solves electrostatic equations in all regions of the device including two narrow regions around the AlGaN/GaN interface with thicknesses of about 3 nm. This model demonstrates how the triangular quantum well is formed around the AlGaN/GaN interface and varies as a function of gate voltages. Using the proposed electrostatic analysis and the treatment proposed by the EPFL HEMT model, the DC current-voltage characteristics are obtained by this model. The results predicted by the model are validated with TCAD simulations and in part with the EPFL HEMT model. The proposed model facilitates the following steps toward obtaining a complete model for small signal and large signal analysis of GaN HEMT.

Review History:

Received: Apr. 12, 2024
Revised: Apr. 28, 2024
Accepted: May, 12, 2024
Available Online: Jul. 01, 2024

Keywords:

Gallium Nitride High Electron Mobility Transistors
Device Modelling
Two-Dimensional Electron Gas
Technology Computer Aided Design

1- Introduction

Recently, GaN-HEMTs have become very popular for high-frequency and high-power switching applications interface [1, 2]. The GaN-HEMT illustrates attractive features distinguishable from GaAs-HEMT. Piezoelectric and spontaneous polarization effects result from the formation of an intrinsic two-dimensional electron gas (2-DEG) [3]. The development of a design-oriented compact model, which takes into account the physical and geometrical device parameters, such as bandgap, polarization effects, and channel length and width, enables the design engineers to analyze the performance of their circuit prior to fabrication. Several popular compact models have been proposed for GaN-HEMT, The MIT virtual source, was a charge-based model originally developed for Si field effect transistor in near ballistic transport conditions and was extended for GaN HEMT simulations by adding some empirical functions [4]. The advanced SPICE model for HEMT (ASM-HEMT) is a surface potential-based compact model [5, 6], which uses regional approximation and smoothing functions to provide continuity between two regions. EPFL HEMT is another charge-based compact model, which was inherited from regular Si FET and tried to merge the essential features of the 2-DEG with the electrostatics during the application of the gate voltage [7-9]. During the last few years, several other models have been proposed to capture GaN HEMT behavior [10-19]. Although the EPFL HEMT model successfully predicts the current-voltage characteristics of the device, a simplifying assumption has been made, It analyzes the device electrostatics in three regions on the device (Metallic gate layer, AlGaN layer, and GaN layer) and neglects the finite width of the 2-DEG layers. Therefore, the EPFL HEMT model cannot predict the detailed band diagram and vertical electric field induced in the device. In this work, we proposed an electrostatic model that takes into account the finite width of the 2-DEG and demonstrates that this model follows the band diagram obtained by TCAD simulations. Here, we solve the Poisson equation in five segments of the device and we derive the band diagram and electric field. Then we extend the proposed model based on the similar approach proposed by the EPFL HEMT model to study and validate the current-voltage characteristics of the device with TCAD simulations and EPFL HEMT model.

2- Device Structure, Parameters and Assumptions

Fig.1 shows the schematic cross-section of the GaN HEMT device used for the model and TCAD simulations. The source and drain regions are distanced from the gate by access regions. The Schottky barrier is formed between the gate and the AlGaN region. The electrostatic solution of the Poisson equation is obtained along the vertical axis shown in Fig. 1, which also specifies the parametric width of various

*Corresponding author's email: shalchian@aut.ac.ir

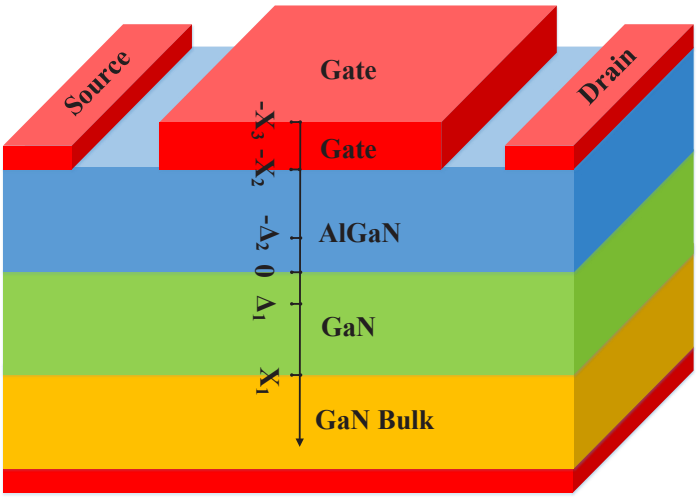

Fig. 1. Shows GaN-HEMT structure in TCAD and determines all symbolic boundary parameters.

layers. Device parameters are defined and listed in Table 1.

The heterostructure is composed of an AlGaN layer grown on top of the GaN layer with an abrupt interface [2, 20]. The gate work function differs from AlGaN electron affinity and the interface turns into a Schottky barrier. The source and drain work function is similar to the AlGaN electron affinity given in Table 1. The AlGaN layer is doped n-type about 5×10^{16} cm^{-3} and gate/AlGaN forms a Schottky barrier. The Thickness of the AlGaN layer is about 20 nm which is thin enough to be considered as a fully depleted layer. The full depletion approximation is valid while applying negative gate voltage and small positive gate voltages below the height of the Schottky barrier. The x-axis is drawn vertically from the gate to the GaN bulk. The axis origin is assumed at the AlGaN/GaN interface where 2-DEG is formed due to the piezoelectric and spontaneous polarization effect.

Two regions are considered on two sides of the origin (Δ_1, Δ_2) to facilitate the development of the model. The GaN bulk is where the electric field goes to zero and X_1 is a boundary around the neutral GaN bulk region. The low-field mobility model, strain, and polarization effects are employed for TCAD simulations [21, 22].

3- Device Model

Recently several valuable models have been proposed for high-frequency FET and HEMT [23-30]. Hereby, a simple and efficient analytical model is introduced in this paper to avoid self-consistent, Poisson–Schrödinger numerical solver to estimate charge, electric field, and potential in the triangular quantum well. This model predicts band-diagram and 2-DEG charge density which are used for high-frequency GaN HEMT models [31-33].

3- 1- Electric field and polarization charge

The differential form of Gauss's law, $\nabla.D = \rho_v$, states that the divergence of the electric displacement field ($\nabla.D$) is equal to volume charge density (ρ_v). The $Al_xGa_{1-x}N$ lattice constant differs from the GaN layer due to the presence of Aluminum mole fraction (x). Bond charges emerge in the $Al_xGa_{1-x}N$ /GaN surface due to strain in the AlGaN layer, are called piezoelectric polarization, and intrinsic charge due to the ionic bond between Al^+ / Ga^+ and N^- are named spontaneous polarization. The electric field and total polarization (ΔP) make the electric displacement field according to $\nabla.\vec{D} = \in \nabla.\vec{\varepsilon} + \nabla.\overrightarrow{\Delta P}$,

$$\in \nabla.\vec{\varepsilon} + \nabla.\overrightarrow{\Delta P} = \rho_v \,. \tag{1}$$

Polarization charges induce a discontinuity in the electric field at the AlGaN/GaN interface. The total amount of polarization charges is about 0.013 C/m^2 taking into consideration the Aluminum mole fraction of 0.15 and the detail parameters listed in Table 2. The $Al_{0.15}Ga_{0.85}N$ and GaN layers are assumed to be doped with $N_D=5\times10^{16}$ and $N_A=1\times10^{16}$ cm^{-3}, respectively. "A" and "D" indices are used to show acceptor and donor type in GaN and AlGaN regions, respectively. The proposed method applies to other doping levels as long as the full depletion approximation is valid. Although AlGaN and GaN show anisotropic behavior, several other works, including [1], consider them isotropic materials.

The electric field in the GaN layer is deduced by considering the depletion region between Δ_1 and X_1, and the electric field in X_1 reaches zero, as shown in (2).

Table 1. DEVICE PARAMETERS [20]

Symbol	Unit	Value and Definitions
x	-	0.15 Aluminum mole fraction
L_G, L_S, L_D	m	10×10^{-6}, 0.1×10^{-6}, 0.1×10^{-6} length of gate, source, and drain
W, t_D	m	10^{-6}, 20×10^{-9} width of the device and the AlGaN thickness
L	m	$L_D+L_S+L_G$ Length of device
χ_D, χ_A	e.V	4.14, 4.31 AlGaN and GaN electron affinity
$\emptyset_G$, $\emptyset_S$, $\emptyset_D$	e.V	5.04, 4.31, 4.31 gate, source, and drain electrode workfunction
N_D, N_A	cm^{-3}	5×10^{16} and 10^{16} AlGaN and GaN doping concentration
N_{CA}, $N_C(AlN)$	cm^{-3}	2.2×10^{18} and 4.1×10^{18} GaN and AlN electron density of state
N_{VA}, $N_V(AlN)$	cm^{-3}	1.16×10^{19} and 2.84×10^{20} GaN and AlN hole density of state
N_{CD}	cm^{-3}	$N_{CD}=(1-x)N_{CA}+xN_C(AlN)$ AlGaN electron density of state
N_{VD}	cm^{-3}	$N_{VD}=(1-x)N_{VA}+xN_V(AlN)$ AlGaN hole density of state
E_{gA}, E_g(AlN)	e.V	3.43 and 6.28 GaN and AlN electron energy gap
E_{gD}	m	$E_{gD}=E_g(AlN)x+(E_{gA}-1.3x)(1-x)$ AlGaN energy gap
ε	V/m	electric field
$\in_0$	F/m	8.85418×10^{-12} Vacuum permittivity
$\in_A$	F/m	$9.5\times\in_0$ GaN permittivity
$\in_D$	F/m	$\in_D=(-0.5x+9.5)\in_0$ AlGaN permittivity
a_A	m	3.189×10^{-10} GaN lattice constant
a_D	m	$a_D=(-0.077x+3.189)\times10^{-10}$ AlGaN lattice constant
Δ_1, Δ_2	m	$12\times a_A$ Widths of 2DEG and polarization layer
DoS_{2D}	$1/m^2v$	$DoS_{2D}=\frac{qm_D^*}{\pi\hbar^2}$ The density of state quantum well
γ_0	$e.v.m^{4/3}$	2.26×10^{-12} Adjustable coefficient

Table 2. POLARIZATION PARAMETERS [1]

Symbol	Unit	Value and Definitions
C_{13}	Gpa	$c_{13}=(5x+103)\times10^{9}$ Elastic constant wurtzite
C_{33}	Gpa	$c_{33}=(-32x+405)\times10^{9}$ Elastic constant wurtzite
e_{31}	C/m^2	$e_{31}=(-0.11x-0.49)$ Piezoelectric coefficient
e_{33}	C/m^2	$e_{33}=(0.73x+0.73)$ Piezoelectric coefficient
P_{SpD}	C/m^2	$P_{SpD}=(-0.052x-0.029)$ AlGaN spontaneous polarization
P_{PeD}	C/m^2	$P_{PeD}=\frac{2(a_A-a_D)}{a_D}\left(e_{31}-e_{33}\frac{C_{13}}{C_{33}}\right)$ AlGaN piezoelectric polarization
P_D	C/m^2	$P_D=P_{SpD}+P_{PeD}$ Total AlGaN polarization
P_A	C/m^2	-0.029 Total GaN polarization
ΔP	C/m^2	$\Delta P=\lvert P_D\rvert-\lvert P_A\rvert$ Total polarization at AlGaN/GaN interface

$$\frac{\mathrm{d}}{\mathrm{d}X}\varepsilon_A(X)=-\frac{qN_A}{\in_A},\quad \varepsilon_A(X_1)=0 \tag{2}$$

The electric field between Δ_1 and X_1 is obtained as:

$$\varepsilon_A(X)=\frac{qN_A(X_1-X)}{\in_A} \tag{3}$$

The relation between volume electron density $n_v(X)$ and sheet electron density N_{ch} in the 2-DEG channel is shown in (4).

$$\int_0^{\Delta_1}\frac{qn_v(X)}{\in_A}\mathrm{d}X=\frac{qN_{ch}}{\in_A} \tag{4}$$

In the 2-DEG channel, the boundary condition is shown in (5) and is obtained by substitution Δ_1 into (3).

$$\varepsilon_{\Delta_1}=\varepsilon_A(X)\big|_{X=\Delta_1}=\frac{qN_A(X_1-\Delta_1)}{\in_A} \tag{5}$$

Taking into account (4) and (5), the electric field in the 2-DEG channel $\varepsilon_{2DEG}(X)$ is obtained:

$$\varepsilon_{2DEG}(X)=\frac{q\left[(X_1-\Delta_1)N_A+N_{ch}\right]}{\in_A} \tag{6}$$

A closed Gaussian surface is assumed between Δ_1 to Δ_2, to obtain the electric field in this region:

$$\Xi_A\,\varepsilon_{\Delta_1}-\in_D\,\varepsilon_{\Delta_2}=q(N_P-N_{ch}) \tag{7}$$

where $N_P=\Delta P/q$. The electric field in Δ_2 is isolated from (7) and given by (8).

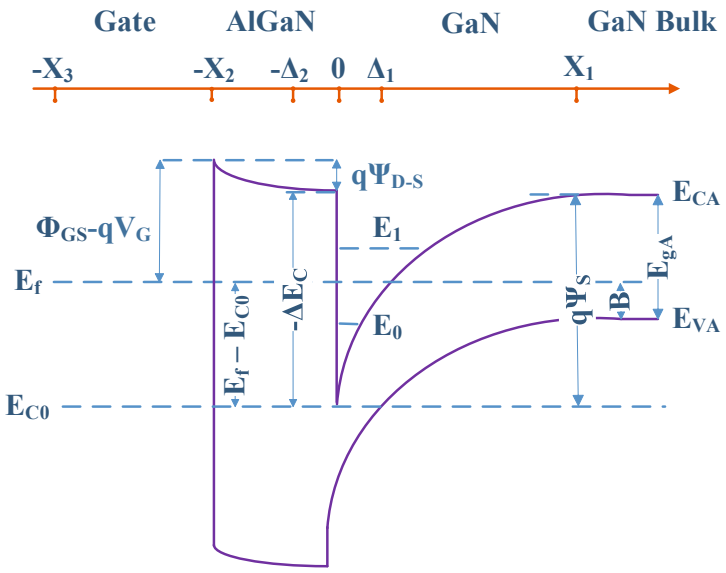

Fig. 2. Energy Band Diagram of GaN-HEMT

$$\varepsilon_{\Delta_2}=\frac{q\left[\left(X_1-\Delta_1\right)N_A+N_{ch}-N_P\right]}{\in_D} \tag{8}$$

To calculate the electric field at $-X_2$, we assume a closed Gaussian surface around $-X_2$. The field at $-X_2$ is a boundary condition for Poisson's equation in the AlGaN region between $-\Delta_2$ to $-X_2$, shown in (9).

$$\begin{aligned}&\frac{\mathrm{d}}{\mathrm{d}X}\,\varepsilon_D\left(X\right)=\frac{qN_D}{\in_D}\\&\varepsilon_{X_2}=\frac{qN_g}{\in_D}\end{aligned} \tag{9}$$

The electric field between $-\Delta_2$ and $-X_2$ into the AlGaN region is solved based on (9) and is shown in (10). The AlGaN region is considered to be fully depleted.

$$\varepsilon_D\left(X\right)=\frac{q\left[\left(X+X_2\right)N_D+N_g\right]}{\in_D} \tag{10}$$

The electric field around $-\Delta_2$ is defined as:

$$\varepsilon_{\Delta_2}=\varepsilon_D\left(X\right)\Big|_{X=-\Delta_2}=\frac{q\left[\left(X_2-\Delta_2\right)N_D+N_g\right]}{\in_D} \tag{11}$$

By equating relations (8) and (11), the charge neutrality relation between N_g, depletion charges, 2-DEG charges, and polarization charges is obtained:

$$N_g=N_A\left(X_1-\Delta_1\right)+N_{ch}-N_P-N_D\left(X_2-\Delta_2\right) \tag{12}$$

Applying an integration, the electric field in all regions is obtained under depletion approximation:

$$\varepsilon(X)=\begin{cases}\varepsilon_G=0 & -X_3\le X<-X_2\\ \varepsilon_D\left(X\right)=\dfrac{q\left[\left(X+X_2\right)N_D+N_g\right]}{\in_D} & -X_2\le X<-\Delta_2\\ \varepsilon_{\Delta_2}=\dfrac{q\left[\left(X_1-\Delta_1\right)N_A+N_{ch}-N_P\right]}{\in_D} & -\Delta_2\le X<0\\ \varepsilon_{2DEG}\left(X\right)=\dfrac{q\left[\left(X_1-\Delta_1\right)N_A+N_{ch}\right]}{\in_A} & 0\le X<\Delta_1\\ \varepsilon_A\left(X\right)=\dfrac{qN_A\left(X_1-X\right)}{\in_A} & \Delta_1\le X\le X_1\end{cases} \tag{13}$$

3- 2- Potential and Band Diagram

The electrostatic potential is calculated by integrating the electric field:

$$\nabla\Psi=-\varepsilon \tag{14}$$

The electric field in the GaN region near the substrate is zero. This is the first boundary condition for the potential:

$$\Psi_A(X_1)=0 \tag{15}$$

Potential at Δ_1 is denoted as a boundary condition for a 2-DEG potential as presented in (16).

$$\Psi_{\Delta_1}=\frac{qN_A(\Delta_1-X_1)^2}{2\in_A} \tag{16}$$

The potential in the 2-DEG layer between Δ_1 and "0" is obtained as:

$$\Psi_{2DEG}(X)= -\frac{q\left[N_A(X_1-\Delta_1)\left(X-\frac{X_1}{2}-\frac{\Delta_1}{2}\right)+N_{ch}(X-\Delta_1)\right]}{\in_A} \tag{17}$$

Ψ_S, the surface potential, is equal to Ψ_{2DEG} at the boundary (X=0) and is presented in (18).

$$\Psi_S=\frac{q\left[N_A\left(X_1^2-\Delta_1^2\right)+2\Delta_1 N_{ch}\right]}{2\in_A} \tag{18}$$

In this relation, the dependence of Ψ_S on gate voltage and drain-source voltage is not explicit. To further explain, in (8) the electrostatics is calculated from the substrate towards the gate, while in (11) it is obtained from the gate towards the substrate. These two equations must be consistent and the charge neutrality emerges from these equalities according to (12). The N_g represents the effect of gate voltage on the N_{ch} and Ψ_S in the charge neutrality equation and in (18). Furthermore, following Gradual Channel Approximation (GCA), we assumed that the variation of the electric field along the channel (y-direction) is much less than the corresponding variation in a vertical direction (x-direction), therefore we first solved the 1-D Poisson equation in the x-direction neglecting drain-source voltage. Next, we will include the effect of V_{DS} on the quasi-Fermi level and implicitly on the charge density at each point of the channel using relation (38). This assumption is valid when the channel length (10 μm, 1 μm), is much longer than the total width of 2DEG and the depletion layer (a few ten nanometers). Next, the potential between "0" to $-\Delta_2$ is obtained as:

$$\Psi_{\Delta_2}(X)=-\frac{qX\left[N_A(X_1-\Delta_1)+N_{ch}-N_P\right]}{\in_D} +\frac{q\left[N_A\left(X_1^2-\Delta_1^2\right)+2\Delta_1 N_{ch}\right]}{2\in_A} \tag{19}$$

This potential is independent of Δ_2. Finally, the potential between $-\Delta_2$ to $-X_2$ is deduced according to (20).

$$\begin{aligned}\Psi_D(X)&=\Psi_{D-S}(X)+\Psi_S\\ \Psi_{D-S}(X)&=\frac{qN_D\Delta_2^2}{2\in_D}\\ &-\frac{q\Delta_2\left[X_2N_D-(X_1-\Delta_1)N_A+N_g-N_{ch}+N_P\right]}{\in_D}\\ &-\frac{qX\left[N_D(X+2X_2)+2N_g\right]}{2\in_D}\end{aligned} \tag{20}$$

The minimum of conduction band energy: $E_C(X)$, follows vacuum-level energy $E_{Vac}(X)$ by a fixed distance called electron affinity (χ). The band bending inside the GaN layer is obtained from (21).

$$\begin{aligned}&E_C|_{GaN}(X)-E_C|_{GaN}(X_1)=\\ &-q\left[\Psi_A(X)-\Psi_A(X_1)\right]\end{aligned} \tag{21}$$

This relation is used to obtain the band diagram at the GaN layer under the depletion approximation. In the AlGaN region, the electron affinity is different from GaN, and the difference is shown as $\Delta\chi=\chi_A-\chi_D$. Taking into consideration, the continuity of the vacuum level, E_C at the boundary of the AlGaN layer is obtained.

$$E_C|_{AlGaN}(X=-\Delta_2)-E_C|_{GaN}(X=\Delta_1)=\Delta\chi \tag{22}$$

Inside the AlGaN layer, the conduction band and valance band both bend in the x-direction to follow the electrostatic potential as described by (23).

$$\begin{aligned}&E_C|_{AlGaN}(X)-E_C|_{AlGaN}(X=-\Delta_2)=\\ &-q\left[\Psi_D(X)-\Psi_D(X=-\Delta_2)\right]\end{aligned} \tag{23}$$

Defining $\Psi_D(-\Delta_2)-\Psi_A(\Delta_1)=\Delta\Psi$ as an equation depending on gate voltage, equation (23) converts to: $E_C|_{AlGaN}(X)-E_C|_{AlGaN}(-\Delta_2)=$.
$-q\left[\Psi_D(X)-\Psi_A(\Delta_1)-\Delta\Psi\right]$

The $q\Psi_A(\Delta_1)=-E_C|_{GaN}(\Delta_1)+E_C|_{GaN}(X_1)$ is obtained from (21) assuming $\Psi_A(X_1)=0$ which is the reference potential of the neutral bulk. After some simplification band bending into the AlGaN region is obtained:

$$\begin{aligned}E_C|_{AlGaN}(X)&=-q\Psi_D(X)\\ &+E_C|_{AlGaN}(-\Delta_2)-E_C|_{GaN}(\Delta_1)\\ &+E_C|_{GaN}(X_1)+q\Delta\Psi\end{aligned} \tag{24}$$

Using (23), (24) is converted to (25).

$$E_C|_{AlGaN}(X) = -q\Psi_D(X) + \Delta\chi + E_C|_{GaN}(X_1) + q\Delta\Psi \qquad (25)$$

Assuming ideal Schottky barrier contact without interface traps, as demonstrated in Fig. 2 the difference between the conduction band around $-X_2$ and Fermi level energy in the gate region is equal to $E_C|_{AlGaN}(-X_2) - E_f = \Phi_G - \chi_D - qV_g$, where $\Phi_G - \chi_D$ is defined as the gate Schottky barrier. Fig. 2 shows the band diagram obtained from this analytical model. The bulk Fermi level energy is defined by $E_f = E_C|_{GaN}(X_1) - E_{gA} + B$, where $B = U_T \ln(N_{VA}/N_A)$. After some simplification, we derive $E_C|_{AlGaN}(-X_2) = \Phi_G - \chi_D - qV_g + E_C|_{GaN}(X_1) - E_{gA} + B$ and next $\Psi_D(-X_2)$ is obtained:

$$\Psi_D(-X_2) = \frac{E_{gA} + \chi_A - B - \Phi_G}{q} + \Delta\Psi + V_g \qquad (26)$$

This relation suggests that the electrostatic potential at the gate boundary with reference to the substrate depends on the gate work function (Φ_G) and GaN layer band gap (E_{gA}). To draw the band diagram, we set the Fermi level at zero ($E_f = 0$) and $E_C|_{GaN}(X_1) = E_{gA} - B$ is obtained. The edges of the conduction bands in AlGaN and GaN are based on (27,28) and the valence band edge is obtained according to $E_V|_{AlGaN(GaN)} = E_C|_{AlGaN(GaN)} - E_{gD(A)}$.

$$E_C|_{GaN}(X) = -q\Psi(X)|_{GaN} + E_{gA} - B \qquad (27)$$

$$E_C|_{AlGaN}(X) = -q\Psi_D(X) + q\Delta\Psi + \Delta\chi + E_{gA} - B \qquad (28)$$

3- 3- Depletion Charge Density model

The width of the depletion layer in the GaN region, X_1, is isolated from (18):

A Gaussian closed surface from Δ_1 to X_1 with a differential Δy length is assumed in the depletion region. The integral form of Gauss law, $Q_b = \oiint \in_A \vec{\varepsilon} \cdot \vec{ds}$, on the closed surface determines the depletion charge.

$$X_1 = \sqrt{\frac{q\Delta_1(N_A\Delta_1 - 2N_{ch}) + 2\in_A \Psi_S}{qN_A}} \qquad (30)$$

The depletion surface charge density is calculated as (31):

$$Q_b = \iint_{top} \in_A \overrightarrow{\varepsilon_{\Delta 1}} \cdot \overrightarrow{ds} + \iint_{bottom} \in_A \vec{0} \cdot \overrightarrow{ds} + \iint_{left} \in_A \overrightarrow{\varepsilon_y} \cdot \overrightarrow{ds} + \iint_{right} \in_A \overrightarrow{\varepsilon_{y+\Delta y}} \cdot \overrightarrow{ds} \qquad (31)$$

Substituting X_1 from (29) into (31) depletion charge density is given by (32).

$$Q_b = \Delta_1 qN_A - \sqrt{qN_A}\sqrt{\Delta_1(N_A\Delta_1 - 2N_{ch})q + 2\in_A \Psi_S} \qquad (32)$$

3- 4- The 2-DEG Channel Charge Density model

Writing (26) as $\Psi_D(-X_2) = A_2 + V_g$ where $A_2 = \frac{E_{gA} + \chi_A - B - \Phi_G}{q} + \Delta\Psi$. The $\Delta\Psi$ is a potential drop over the 2-DEG layer which is small versus $\frac{E_{gA} + \chi_A - B - \Phi_G}{q}$. Also (20) is written as $\Psi_D(-X_2) = \Psi_{D-S}(-X_2) + \Psi_S$ where

$$\Psi_{D-S}(-X_2) = B_2 + \frac{q\Delta_2 X_1 N_A}{\in_D} \text{ and } B_2 = \frac{qN_D\Delta_2^2}{2\in_D} - \frac{q\Delta_2 X_2 N_D}{\in_D} - \frac{q\Delta_2 N_g}{\in_D} + \frac{q\Delta_2 N_{ch}}{\in_D} + \frac{qX_2 N_g}{\in_D} - \frac{q\Delta_2\Delta_1 N_A}{\in_D} - \frac{q\Delta_2 N_P}{\in_D} + \frac{qN_D X_2^2}{2\in_D}$$

The N_g and X_1 are given by (12) and (29) which are substituted in $\Psi_{D-S}(-X_2)$. Finally, N_{ch} is isolated from $\Psi_D(-X_2) = A_2 + V_g = \Psi_{D-S}(-X_2) + \Psi_S$. Applying $Q_{ch} = -qN_{ch}$ the 2-DEG charge is written as:

$$Q_{ch} = \sqrt{2}\sqrt{-qN_A C_b\Delta_1 V_g + E_2 + qN_A(C_b\Delta_1 + \in_A)\Psi_S} + F_2 - (V_g - \Psi_S)C_b \qquad (33)$$

where $C_b = \frac{\in_D}{X_2}$ is the capacitance per unit area in the AlGaN region. Other variables C_2, D_2, E_2, F_2 are defined in (34)

$$\begin{aligned} C_2 &= N_A^2 X_2\Delta_1^2\Delta_2 q^2 - N_A X_2\Delta_1 q^2 \times(\Delta_2 - X_2)(-X_2 N_D + N_D\Delta_2 - N_P) \\ D_2 &= q[-N_D\Delta_2^2 + (N_A\Delta_1 + 2X_2 N_D + N_P)\Delta_2 - X_2^2 N_D - N_P X_2] \\ E_2 &= \frac{C_2}{X_2^2} - qN_A C_b\Delta_1(A_2 - B_2) \\ F_2 &= \frac{D_2}{X_2} - (A_2 - B_2)C_b \end{aligned} \qquad (34)$$

Relation (33) suggests a parabolic relation between on Q_{ch} and $\sqrt{\Psi_S}$, Therefore Ψ_S can be written as:

$$\Psi_S = \frac{-\sqrt{\begin{matrix} q^2(C_b\Delta_1 + \in_A)^2 N_A^2 \\ -2\left[C_b(-Q_{ch} + F_2)\Delta_1 - \in_A(C_b V_g - F_2 + Q_{ch})\right]qC_b N_A \\ +2C_b^2 E_2 \end{matrix}}}{C_b^2} + \frac{2C_b^2 V_g + (2\Delta_1 qN_A - 2F_2 + 2Q_{ch})C_b + 2qN_A\in_A}{C_b^2} \qquad (35)$$

Assuming Δ_1 and Δ_2 having zero width, (33) turns to a simplified form used in the EPFL HEMT model (32) in [7].

To obtain the sheet charge concentration in subbands of the conduction band, we should take into consideration the 2D density of states: $DoS_{2D} = m^* / \pi\hbar^2$ where m* is the electron effective mass and $\hbar$ is reduced Plank constant, and the probability of occupation of the first subband (E_0) according to Fermi-Dirac statistics, which leads to:

$$N_{ch} = DoS_{2D} U_T \ln\left(1+e^{\frac{E_f - E_0}{qU_T}}\right) \tag{36}$$

The existence of a triangular quantum well at the interface of AlGaN and GaN suggests the following relation between E_0, N_{ch} and E_{C0} [7].

$$E_0 - E_{C0} = \gamma_0 N_{ch}^{\frac{2}{3}} \tag{37}$$

Besides, the distance between the Fermi level in the quantum well and lower subband can be written based on the electrostatic relation as depicted in Fig. 2:

$$E_f - E_0 = q\Psi_S - qV_{ap} - E_{gA} + B - \left(E_0 - E_{C0}\right) \tag{38}$$

V_{ap} is the voltage applied to the channel, V_{ap}(Source)=0 and V_{ap}(Drain)=$V_{DS.}$ Substituting (37) and (38) in (36), a nonlinear equation is obtained which relates N_{ch} to V_{ap} and Ψ_S.

$$N_{ch} = DoS_{2D} U_T \ln\left[1+\exp\left(\frac{\Psi_S - V_{ap} - \hat{E}_{gA} + \hat{B} - \hat{\gamma}_0 N_{ch}^{\frac{2}{3}}}{U_T}\right)\right]. \tag{39}$$

Relation (39) shows how N_{ch} varies with the surface potential and with the channel voltage. The next step is solving (35) and (39) together assuming $\hat{E}_{gA}$, $\hat{B}$ and $\hat{\gamma}_0$ to have the voltage dimension and obtaining the charge density at the source side Q_S and the drain side Q_D of the channel. Then, forward and reverse currents, I_f and I_r, are calculated using EKV formalism [34].

$$I_r = Q_D{}^2 - Q_D, I_f = Q_S{}^2 - Q_S. \tag{40}$$

The drain current is derived from $I_d = I_f - I_r$ [7, 20].

4- Simulation Results and Discussion

The electric field along the X direction for various gate voltages is illustrated in Fig. 3. (a). The result obtained by the model shows good agreement with TCAD simulation. The model follows TCAD results in the negative gate voltages but deviates slightly from TCAD in positive gate voltages. The difference between the model and TCAD is the result of a "full depletion approximation" where the AlGaN layer is not fully depleted in positive gate voltages. The error of considering this assumption remains small when the gate voltage is limited to the height of the Schottky barrier about 0.8 V. The width of the depletion region in the AlGaN region decreases when gate voltage increases. The electric field in the gate electrode is zero, and the electric field is negative in the AlGaN region. There is a spike of about 1.5 MV/cm around the 2-DEG region at V_G=0.5 V, which is predicted by the proposed model and the electric field decreases sharply in the AlGaN/GaN interface around Δ_1 and smoothly goes to zero towards the substrate.

Fig. 3(b) shows the potential plotted along the X-axes. It clearly illustrates a sharp peak around X=0 within the Δ_1 interval where 2-DEG is formed. Fig. 3 (b) depicts how the proposed model facilitates and how the potential varies in response to gate voltage and the 2-DEG formation. Beyond X_1 where GaN bulk is neutral electric field goes to zero and we consider the potential as a reference potential. The reference potential can be defined in various ways. For TCAD, this is always the intrinsic Fermi potential ψ_I=-(E_f-E_i)/q, which has a negative value of about -1.6V for the substrate doping concentration (N_A).

Fig 4. (a) compares the edges of the conduction band and the valance band calculated by (27) and (28) with the TCAD simulation result. Fig 4(b), shows a similar band diagram, magnified at the Matal/AlGaN/GaN interface region. It indicates perfect agreement between the proposed analytical model and the TCAD simulation. The quantum well around X=0 predicted by our model exactly follows the TCAD results according to Fig. 4 (b). To calibrate the model with experimental data, we used "Δ_1" and "Δ_2" as fitting parameters and we obtained the best fitting values for both parameters as $12 \times a_A = 3.8$ nm, where a_A is the GaN lattice constant listed in Table 1. The results have been validated for the range of fraction mole from 0.15 to 0.3, where the AlGaN/GaN interface is smooth enough to avoid dislocations.

The proposed model uses the thickness of 2DEG (Δ_1) and polarization layer (Δ_2) to derive the electric field and potential. The proposed model reverts to the EPFL HEMT model if we neglect the thickness of those layers and assume the 2DEG and polarization layers as charge sheets at the GaN/AlGaN interface.

Fig. 5 (a) and (b) compare the I_D-V_G and I_D-V_D characteristics obtained by the proposed model with the EPFL HEMT model and indicate that both models follow the TCAD simulation results in all operating regions. TCAD results show that the drain current decreases beyond the gate voltage of 0.8 V since some of the carriers emit to the gate instead of the drain from the AlGaN Schottky barrier. The Schottky barrier height is the difference between the gate work function and the semiconductor electron affinity. The AlN semiconductor layer shows an electron affinity of 0.6

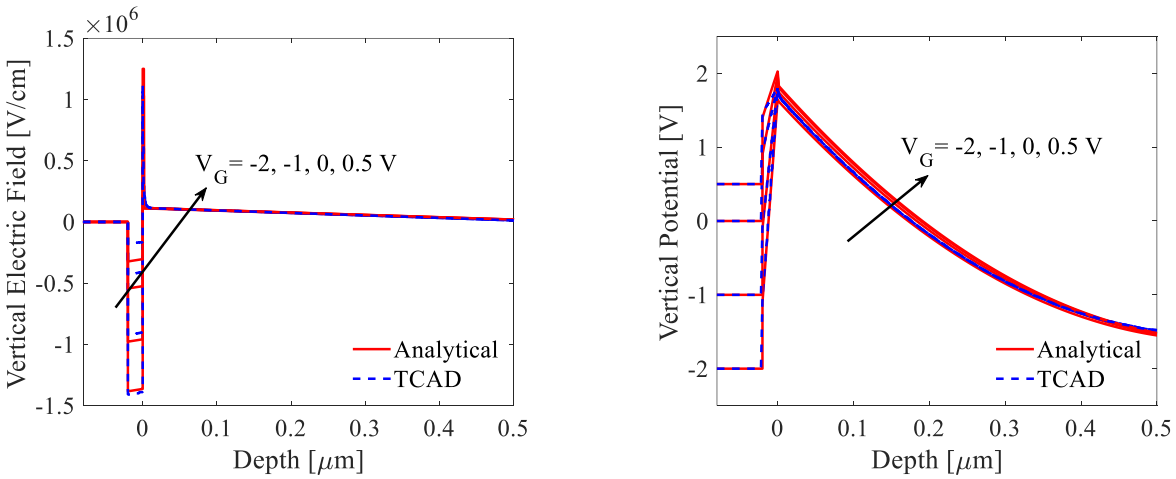

(a) (b)

Fig. 3. (a) Vertical electric field and (b) potential from gate to bulk

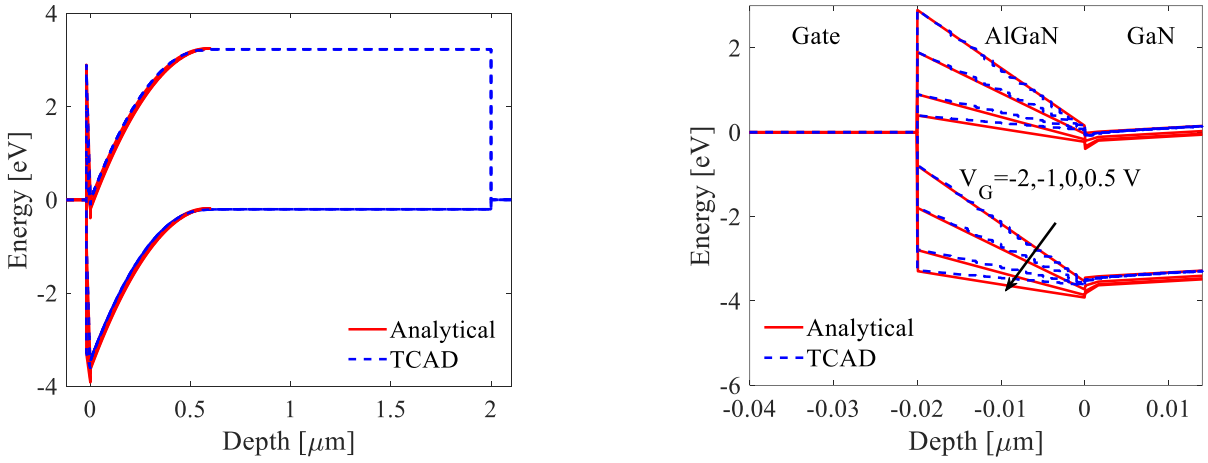

(a) (b)

Fig. 4. (a) Energy band diagram of GaN HEMT device at source and drain from the gate to the bulk (b) magnified band diagram around the 2-DEG layer.

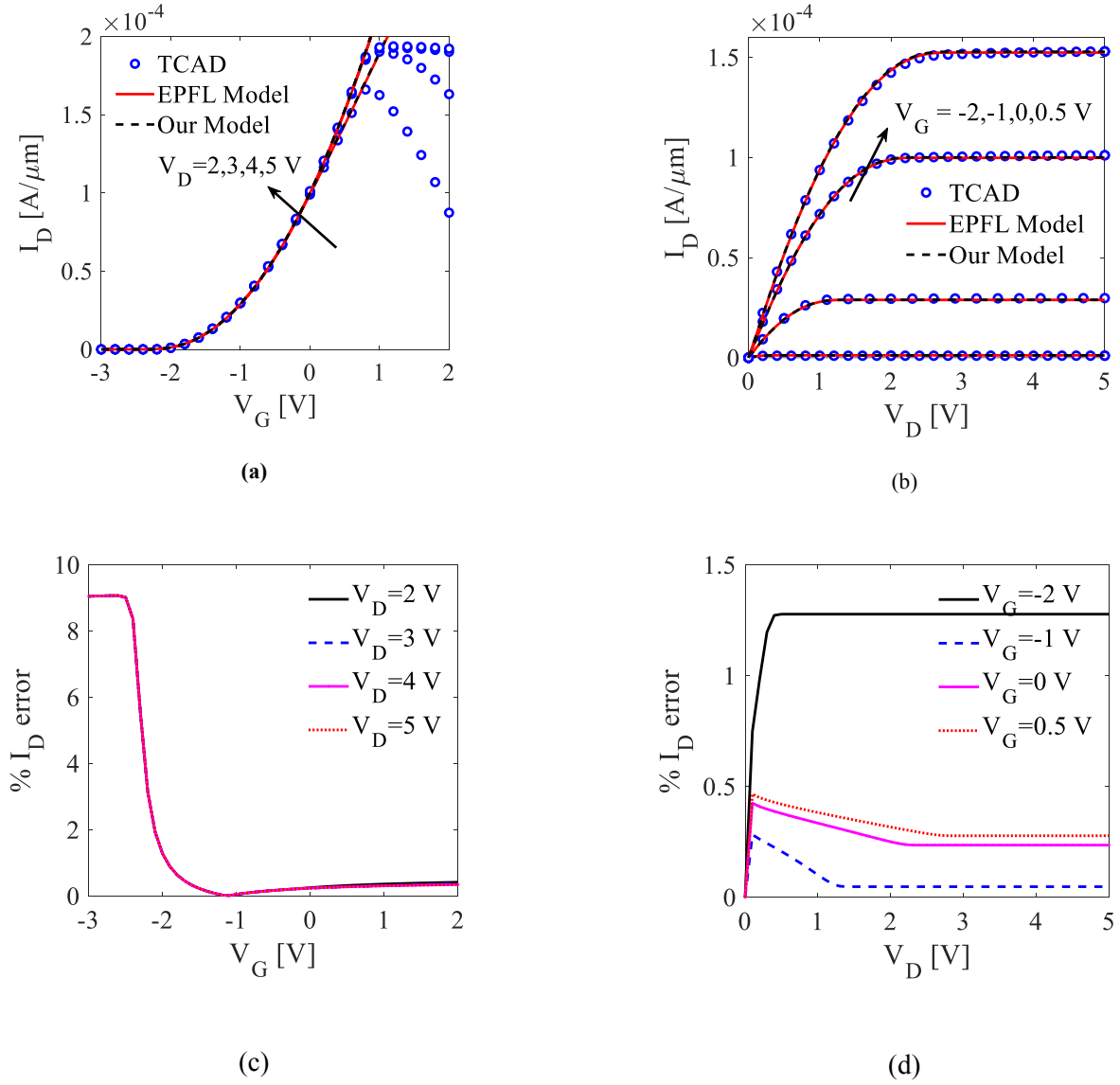

Fig. 5. (a) ID-VG, (b) ID-VD characteristics obtained from the proposed model compared with EPFL HEMT model and TCAD simulations. (c) and (d) indicate the error % in ID-VG and ID-VD respectively between the proposed model and the EPFL model.

eV [35] leading to an increase in Schottky barrier height. The results of the EPFL HEMT model and our model shown in Fig.5 (a) and (b) are close to each other. The relative error in percent in I_D-V_G and I_D-V_D estimation is shown in Fig. 5 (c) and (d). These diagrams show that the EPFL HEMT model shows a little deviation of 1.2% in the above threshold and up to 9% in the subthreshold operating region from the proposed model. From the results of Fig. 5, we have also calculated the rough amount of total error using the root-mean-square (RMS) relative values for I_D-V_G indicating errors in percent of about 2.946, 2.943, 2.941, and 2.941 for V_D= 2, 3, 4 and 5 V respectively. The RMS errors for I_D-V_D are 1.25, 0.099, 0.277, and 0.324 in percent for V_G=-2, -1, 0, and 0.5 V respectively.

5- Conclusion

A novel analytical model is introduced to calculate the DC characteristics including the electric field in different GaN-HEMT regions. The widths of the 2DEG layer and polarizations at the AlGaN/GaN interface significantly influence the electric field distribution. The model employs "full depletion approximation" in the AlGaN region. The model shows little deviation from TCAD results in positive gate voltage due to full depletion approximation. However, the error arising from this approximation is negligible for a narrow AlGaN layer. The potential and energy band diagram follow TCAD simulation in all device regions under various gate voltages even around the 2-DEG region. The electric field, follows TCAD and the proposed model predicts the spiking shape around the AlGaN/GaN interface at about 1.5 MV/cm at V_G= 0.5V. The proposed model converts to the EPFL HEMT model, if we neglect the thickness of 2DEG and polarization layers.

References

[1] O. Ambacher, J. Smart, J. Shealy, N. Weimann, K. Chu, M. Murphy, W. Schaff, L. Eastman, R. Dimitrov, L. Wittmer, Two-dimensional electron gases induced by spontaneous and piezoelectric polarization charges in N-and Ga-face AlGaN/GaN heterostructures, Journal of applied physics, 85(6) (1999) 3222-3233.

[2] D. Delagebeaudeuf, N.T. Linh, Metal-(n) AlGaAs-GaAs two-dimensional electron gas FET, IEEE Transactions on Electron Devices, 29(6) (1982) 955-960.

[3] M.N. Yoder, Wide bandgap semiconductor materials and devices, IEEE Transactions on Electron Devices, 43(10) (1996) 1633-1636.

[4] U. Radhakrishna, T. Imada, T. Palacios, D. Antoniadis, MIT virtual source GaNFET-high voltage (MVSG-HV) model: A physics based compact model for HV-GaN HEMTs, physica status solidi (c), 11(3-4) (2014) 848-852.

[5] A. Dasgupta, S. Ghosh, Y.S. Chauhan, S. Khandelwal, Asm-hemt: Compact model for gan hemts, in: 2015 IEEE International Conference on Electron Devices and Solid-State Circuits (EDSSC), IEEE, 2015, pp. 495-498.

[6] S.A. Ahsan, S. Ghosh, S. Khandelwal, Y.S. Chauhan, Physics-based multi-bias RF large-signal GaN HEMT modeling and parameter extraction flow, IEEE Journal of the Electron Devices Society, 5(5) (2017) 310-319.

[7] F. Jazaeri, J.-M. Sallese, Charge-based EPFL HEMT model, IEEE Transactions on Electron Devices, 66(3) (2019) 1218-1229.

[8] F. Jazaeri, M. Shalchian, J.-M. Sallese, Transcapacitances in EPFL HEMT model, IEEE Transactions on Electron Devices, 67(2) (2019) 758-762.

[9] M. Allaei, M. Shalchian, F. Jazaeri, Modeling of short-channel effects in GaN HEMTs, IEEE Transactions on Electron Devices, 67(8) (2020) 3088-3094.

[10] A. Chalechale, M. Shalchian, F. Jazaeri, Transient analysis of donor-like surface traps in GaN HEMTs, AUT Journal of Electrical Engineering, 54(2 (Special Issue)) (2022) 387-396.

[11] H. Luo, W. Hu, Y. Guo, On large-signal modeling of GaN HEMTs: Past, development, and future, Chip, (2023) 100052.

[12] B.J. Touchaei, M. Shalchian, Modeling GaN-HEMT Electrostatic Band Diagram under full depletion approximation, in: 2023 5th Iranian International Conference on Microelectronics (IICM), IEEE, 2023, pp. 134-138.

[13] N. Islam, M.F.P. Mohamed, N. Ahmad, M.M. Isa, A.F. Abd Rahim, K. Ahmeda, Analytical Modeling of Depletion-Mode MOSHEMT Device for High-Temperature Applications, IEEE Access, (2024).

[14] Y. Liu, X. Liu, X. Li, H. Yuan, Analytical Model and Safe-Operation-Area Analysis of Bridge-Leg Crosstalk of GaN E-HEMT Considering Correlation Effect of Multi-Parameters, IEEE Transactions on Power Electronics, (2024).

[15] P. Sriramani, N. Mohankumar, Y. Prasamsha, Drain current sensitivity analysis using a surface potential-based analytical model for AlGaN/GaN double gate MOS-HEMT, Micro and Nanostructures, 185 (2024) 207720.

[16] M. Faizan, K. Han, X. Wang, M.Z. Yousaf, Mathematical Model-Based Analysis and Mitigation of GaN Switching Oscillations, IEEE Access, (2024).

[17] R.P. Martinez, M. Iwamoto, J. Xu, C. Gillease, S. Cochran, M. Culver, A. Cognata, N.S. Wagner, P. Pahl, S. Chowdhury, Assessment and Comparison of Measurement-Based Large-Signal FET Models for GaN HEMTs, IEEE Transactions on Microwave Theory and Techniques, (2024).

[18] Q. He, H. Wang, M. Xiao, Y. Zhang, K. Sheng, F. Udrea, Numerical Simulation and Analytical Modeling of Multichannel AlGaN/GaN Devices, IEEE Transactions on Electron Devices, 71(3) (2024) 1710-1717.

[19] X. Liu, S. Shafie, M.A.M. Radzi, N. Azis, A.H.A. Karim, Modelling and mitigating oscillation in E-mode

GaN HEMT: A simulation-based approach to parasitic inductance optimization, Microelectronics Reliability, 152 (2024) 115293.

[20] B.J. Touchaei, M. Shalchian, Non-Quasi-Static Intrinsic GaN-HEMT Model, IEEE Transactions on Electron Devices, 69(12) (2022) 6594-6601.

[21] A. Bykhovski, B. Gelmont, M. Shur, The influence of the strain-induced electric field on the charge distribution in GaN-AlN-GaN structure, Journal of applied physics, 74(11) (1993) 6734-6739.

[22] J. Albrecht, R. Wang, P. Ruden, M. Farahmand, K. Brennan, Electron transport characteristics of GaN for high temperature device modeling, Journal of Applied Physics, 83(9) (1998) 4777-4781.

[23] M. Movahhedi, A. Abdipour, Efficient numerical methods for simulation of high-frequency active devices, IEEE Transactions on Microwave Theory and Techniques, 54(6) (2006) 2636-2645.

[24] V. Joshi, A. Soni, S.P. Tiwari, M. Shrivastava, A comprehensive computational modeling approach for AlGaN/GaN HEMTs, IEEE Transactions on Nanotechnology, 15(6) (2016) 947-955.

[25] I.R. Rahman, M.I. Khan, M. Mahdia, Q.D. Khosru, Analytical modeling of electrostatic characteristics of enhancement mode GaN double channel HEMT, in: 2018 IEEE 13th Nanotechnology Materials and Devices Conference (NMDC), IEEE, 2018, pp. 1-4.

[26] I.R. Rahman, M.I. Khan, Q.D. Khosru, A rigorous investigation of electrostatic and transport phenomena of GaN double-channel HEMT, IEEE Transactions on Electron Devices, 66(7) (2019) 2923-2931.

[27] N. Modolo, S.-W. Tang, H.-J. Jiang, C. De Santi, M. Meneghini, T.-L. Wu, A novel physics-based approach to analyze and model E-mode p-GaN power HEMTs, IEEE Transactions on Electron Devices, 68(4) (2020) 1489-1494.

[28] I. Berdalović, M. Poljak, T. Suligoj, Modelling of electrostatics and transport in GaN-based HEMTs under non-equilibrium conditions, in: 2021 44th International Convention on Information, Communication and Electronic Technology (MIPRO), IEEE, 2021, pp. 74-79.

[29] M.G. Carpenter, P.H. Aaen, C.M. Snowden, Quasi-2-D Physical Modeling of GaN Microwave HEMTs for RF Applications, IEEE Transactions on Electron Devices, 69(11) (2022) 6002-6009.

[30] V.N. Kumar, M. Povolotskyi, D. Vasileska, Modeling electrostatics and low-field electron mobility of GaN FinFETs, IEEE Transactions on Electron Devices, 69(9) (2022) 4835-4842.

[31] B.J. Touchaei, M. Shalchian, A compact Non-Quasi-Static small-signal model for GaN HEMT, Microelectronics Journal, (2024) 106199.

[32] V. Vadalà, A. Raffo, A. Colzani, M.A. Fumagalli, G. Sivverini, G. Bosi, G. Vannini, On the Extraction of Accurate Non-Quasi-Static Transistor Models for $ E $-Band Amplifier Design: Learning From the Past, IEEE Transactions on Microwave Theory and Techniques, (2024).

[33] H. Lee, H.-G. Park, V.-D. Le, V.-P. Nguyen, J.-M. Song, B.-H. Lee, J.-D. Park, X-band MMICs for a Low-Cost Radar Transmit/Receive Module in 250 nm GaN HEMT Technology, Sensors, 23(10) (2023) 4840.

[34] C.C. Enz, E.A. Vittoz, Charge-based MOS transistor modeling: the EKV model for low-power and RF IC design, John Wiley & Sons, 2006.

[35] M.E. Levinshtein, S.L. Rumyantsev, M.S. Shur, Properties of Advanced Semiconductor Materials: GaN, AIN, InN, BN, SiC, SiGe, John Wiley & Sons, 2001.

HOW TO CITE THIS ARTICLE

B. Jafari Touchaei, M. Shalchian. Analytical Modeling of GaN-HEMT Considering Finite Width of Two-Dimensional Electron Gas . AUT J Electr Eng, 56(3) (2024) 407-418.

DOI: 10.22060/eej.2024.23101.5588